

# Undulations of lamellar liquid crystals in cells with finite surface anchoring near and well above the threshold

B. I. Senyuk, I. I. Smalyukh, and O. D. Lavrentovich\*

*Liquid Crystal Institute and Chemical Physics Interdisciplinary Program, Kent State University, Kent, Ohio 44242, USA*

(Received 19 April 2006; published 31 July 2006)

We study the undulations instability, also known as the Helfrich-Hurault or layers buckling effect, in a cholesteric liquid crystal confined between two parallel plates and caused by an electric field applied along the normal to layers. The cholesteric pitch is much smaller than the cell thickness but sufficiently large for optical study. The three-dimensional patterns of the undulating layers in the bulk and at the surfaces of the cells are determined by fluorescence confocal polarizing microscopy. We demonstrate that the finite surface anchoring at the bounding plates plays a crucial role in the system behavior both near and well above the undulations threshold. The displacement of the layers immediately above the undulation threshold is much larger than the value expected from the theories that assume an infinitely strong surface anchoring. We describe the experimentally observed features by taking into account the finite surface anchoring at the bounding plates and using Lubensky-de Gennes coarse-grained elastic theory of cholesteric liquid crystals. Fitting the data allows us to determine the polar anchoring coefficient  $W_p$  and shows that  $W_p$  varies strongly with the type of substrates. As the applied field increases well above the threshold value  $E_c$ , the layers profile changes from sinusoidal to the sawtooth one. The periodicity of distortions increases through propagation of edge dislocations in the square lattice of the undulations pattern. At  $E \approx 1.9E_c$  a phenomenon is observed: the two-dimensional square lattice of undulations transforms into the one-dimensional periodic stripes. The stripes are formed by two sublattices of defect walls of parabolic shape. The main reason for the structure is again the finite surface anchoring, as the superposition of parabolic walls allows the layers to combine a significant tilt in the bulk of the cell with practically unperturbed orientation of layers near the bounding plates.

DOI: [10.1103/PhysRevE.74.011712](https://doi.org/10.1103/PhysRevE.74.011712)

PACS number(s): 61.30.Eb, 61.30.Hn, 61.30.Jf

## I. INTRODUCTION

Phases with one-dimensional (1D) periodic structure composed of fluid layers can be found in a wide variety of physical and chemical systems. The well-known experimental realizations are smectic and cholesteric liquid crystals (LCs), lyotropic lamellar phases, melted block copolymers, magnetic films, and ferrofluids, see, for example [1–3]. They exhibit a variety of physical phenomena of both fundamental and applied interest. As the periodic structure is featured only in one direction, the layers can easily bend in response to external fields and boundary conditions. The morphology of ensuing configurations is rich and includes dislocations, disclinations, dispirations and their assemblies, chevrons and other types of tilt boundaries, focal conic domains, periodic undulations, etc. The most studied type of structural instability that does not alter topology of the uniform ground state is the so-called undulations or buckling of layers, also known as the Helfrich-Hurault effect. Originally, the effect has been described by Helfrich for a flat cholesteric LC sample in which the orientation of layers is set parallel to the bounding plates [4,5]. When the external electric field is applied across the cell, the layers tend to reorient parallel to the field; free rotation is hindered by the surface anchoring forces. Assuming that the boundary layers remain clamped by an infinitely strong surface anchoring, Helfrich demonstrated that above some threshold field  $E_c$ , the layers should experience a sinusoidal periodic tilt; the tilt is maximum in the middle of the cell and vanishes at the boundaries. Clark and Meyer [6] and

Delaye, Ribotta, and Durand [7] observed that undulations can be caused also by a dilative mechanical stress: the layers tilt to increase their effective thickness measured along the normal to the cell, which allows them to fill the additional space created between the plates. In the mechanical effect, the undulations are metastable. The equilibrium could be reached through nucleation and propagation of dislocations, but their appearance might be hindered by high energy barriers.

Experimental studies of undulations are difficult, especially in the three-dimensional (3D) systems, as the appropriate technique should be nondestructive and provide information about the local structure of layers and its variation not only in the  $xy$  plane of a flat sample but also along the  $z$  axis, normal to the bounding plates. Most of the available techniques produce only spatially integrated information about the 3D structure, see, e.g., [8]. In this work, we use the fluorescence confocal polarizing microscopy (FCPM) [9,10] to explore experimentally a fully 3D pattern of undulations, both near the threshold and well above it. As the system to study, we have chosen a cholesteric LC in which the undulations are caused by the electric field. In the cholesteric LC, the local director rotates around a single axis remaining perpendicular to this axis and thus forming a helicoidal structure with a pitch  $p$ . We chose the material with  $p \approx 5 \mu\text{m}$  much smaller than the thickness  $d$  of the LC cells (in the range 50–70  $\mu\text{m}$ ) and the period of ensuing undulations, so that the cholesteric LC can be described as a lamellar LC [1,11]. At the very same time,  $p$  is sufficiently large to allow one a direct and detailed optical visualization [12] of the layers and their undulations not only in the plane of a sample but also across the sample. We study a quasistatic regime, when the

\*Corresponding author. Email address: odl@lci.kent.edu

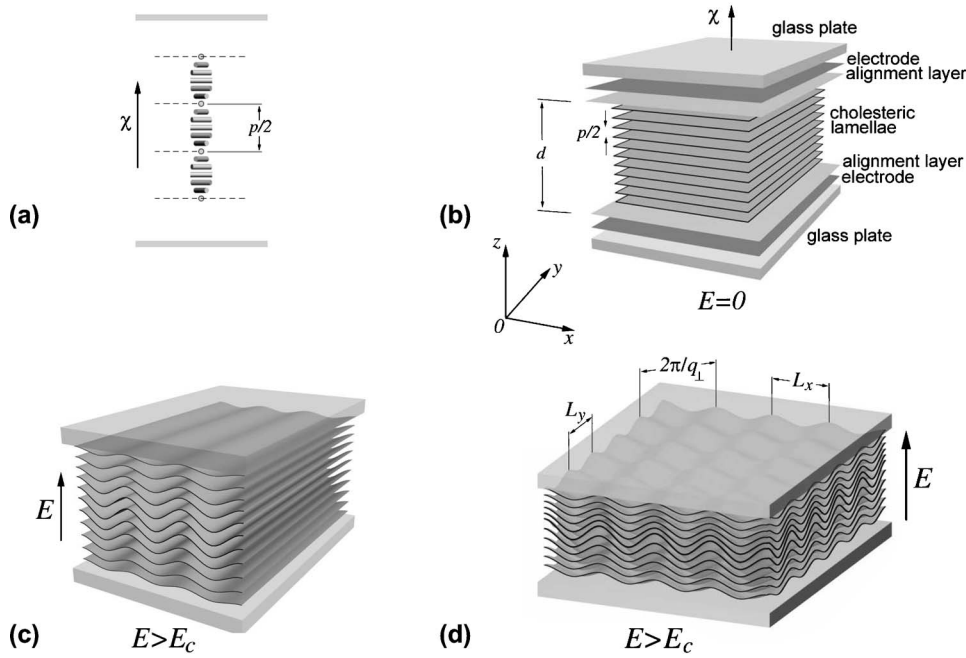


FIG. 1. (a) Schematic representation of a cholesteric layered system with the layer thickness  $p/2$ ;  $p$  is the cholesteric pitch; (b) LC cell in zero electric field  $E=0$ ;  $d$  is the cell thickness; and  $\chi$  is the helix axis. Periodic distortions above the threshold field  $E > E_c$ : a hypothetical 1D pattern (c), or a 2D square lattice (d).

field increase rate is much lower than the rate of undulations growth.

We demonstrate that the anisotropic forces of surface anchoring responsible for layers alignment play a crucial role at the onset and development of undulations. A finite surface anchoring strength leads to the lower threshold of undulation instability, larger layers' displacements, and tilts in the bulk. When the field increases well above the threshold, the sinusoidal undulations first evolve into a chevron or zigzag pattern with an increased period [similarly to the two-dimensional (2D) case [13–16] and in accord with the recent theory by Singer for 3D [17]]. This transformation from a single Fourier mode into a zigzag pattern is accompanied by a weakened dependence of the layers shape on the vertical  $z$ -coordinate; the finite surface anchoring facilitates the transformation as the layers become strongly tilted not only in the bulk but also at the surfaces. Well above the threshold the pattern transforms again, but not into the anticipated pattern of parabolic focal conic domains: rather unexpectedly, the 2D square pattern of zigzag undulations transforms into a 1D periodic pattern formed by a system of parabolic walls (PWs), which has never been described before. The PWs balance the dielectrically induced layers reorientation in the bulk and surface anchoring at the boundaries, managing to avoid unfavorable tilted orientation of layers near the surfaces, but allowing it in the bulk.

The outline of this paper is as follows. In Sec. II, after a short review of the field, we present the basic theory of undulations in a 3D lamellar system with finite surface anchoring. Section III describes materials and the experimental techniques. We discuss our main results and draw conclusions in Secs. IV and V, respectively.

## II. LAYERS UNDULATIONS IN CHOLESTERIC LAMELLAE

### A. Undulations instability in layered systems

Since pioneering works of Helfrich [4,5], layers undulations under mechanical, temperature, electric, and magnetic

field action as well as shear [18,19] have been studied for smectic  $A$  [6,7,13,14,17,20–24], smectic  $C$  [25], and cholesteric [15,16,26–34] LCs, aqueous DNA solutions [35], lyotropic lamellar LCs [19,36], lamellae-forming block copolymers [18,37,38], LC elastomers [39,40], ferrofluids [41], ferrimagnets [42,43], and multiwall carbon nanotubes [44]. Wrinkling of thin elastic sheets [45] and undulations of columnar LC phases [46] might also be added to the list.

The original model assumed that the undulations develop only along one direction in the plane of the sample, Fig. 1(c). Such a model would describe a periodic buckling in 2D systems such as magnetic stripe phases [43], ferrofluids [41], or cholesteric “fingerprint” textures [15,16]. At the onset of instability, the layers profile in the bulk is well-described by a sinusoidal line [13]. As the field increases, the sinusoidal profile (a) evolves into the sawtooth (called also zigzag, chevron, or kink) structure and (b) increases its periodicity [13]. These trends have been observed in experiments with (effectively 2D) ferrimagnetic films [43] and 2D LC samples, both in part (a) [14–16] and (b) [16].

Delrieu [31] demonstrated that in a 3D system with no special unidirectional treatment of the bounding plates, the pattern of undulations is of a square lattice type, Fig. 1(d), in agreement with experiments [21,26,28,32]. The recent theory by Singer [17] predicts that the layer's shape changes similarly to the 2D case, namely, it evolves from the sinusoidal to zigzag form as the field increases much above the threshold. The difference between the behavior of the square lattice in the 3D sample and one-directional undulations in the 2D sample might be substantial, however. For example, Fukuda and Onuki [22] demonstrated that the dynamics of transient pattern formed by a sudden field increase above the undulation threshold might be much slower in the one-directional pattern of undulations.

A spectacular departure from the sinusoidal-chevron scenario for dilation-induced undulations in smectic  $A$  has been discovered by Rosenblatt, Pindak, Clark, and Meyer much

above the threshold [47]. The layers change their topology and fold into a square lattice of parabolic focal conic domains (PFCDs). The layers are in the form of Dupin cyclides for which the focal surfaces degenerate into 1D singularities, in this case a pair of parabolaes that pass through each other's focus [3]. The PFCDs are capable of relaxing the dilative strain because the layers within the PFCD are tilted and also because layers within a certain portion of the PFCD are multiply connected (so that the same layer crosses the vertical line drawn between the two bounding plates three times thus, effectively, filling the space added by dilation). Similar PFCD lattices have been observed in temperature- or dilation-induced undulation patterns in lyotropic LCs [48,49]. However, Asher and Pershan [49] pointed out that only a portion of polygonal textures they observed can be identified as PFCD lattices; many other textures have a more complex structure that cannot be deciphered by a standard PM technique used by them and other researchers.

In the early works, starting from the classic Helfrich-Hurault theory of the undulations, it was assumed that deformation of the layers at the cell boundaries is zero. In other words, the surface anchoring was assumed to be infinitely strong, thus setting restrictions on the values of wave vectors in the undulations pattern. This assumption is not universally valid, as was demonstrated for 2D cholesteric lamellar samples [15,16]. Finite anchoring and the possibility to tilt the layers at the substrate substantially modify the onset and development of undulations; for example, layers displacements are much larger while the threshold is lower than one could expect from the classic theories with an infinitely strong surface anchoring. Below, we extend the 2D model of undulations in a cell with the finite anchoring proposed in Refs. [15,16], to the fully 3D case.

### B. Cholesteric lamellae in electric field

We consider a cholesteric LC confined between two flat substrates separated by the distance  $d \gg p$ ; the helical axis  $\hat{\chi}$  is normal to the substrates, Figs. 1(a) and 1(b). In the presence of the electric field  $\mathbf{E}$  the free energy density of the system acquires a dielectric contribution  $-\varepsilon_0 \varepsilon_a (\hat{\chi} \cdot \mathbf{E})^2 / 2$ , where  $\varepsilon_a = 2\varepsilon_\perp (\varepsilon_\perp - \varepsilon_\parallel) / (\varepsilon_\parallel + \varepsilon_\perp)$  [50,51] is an effective dielectric anisotropy calculated with respect to  $\hat{\chi}$  [16],  $\varepsilon_\parallel$  and  $\varepsilon_\perp$  are the dielectric permittivities measured in nontwisted material parallel and perpendicularly to the director  $\mathbf{n}$ , respectively. In the experiment (see Sec. III), we chose a material in which the dielectric anisotropy is weak,  $\varepsilon_\parallel - \varepsilon_\perp < \varepsilon_\perp$ , to mitigate the effects of nonlocality of the electric field [24]. When the typical scale of distortions is large as compared to  $p$ , one can neglect the specific twisted structure of the cholesteric LC and describe it as a lamellar medium [1,11] with the free energy density [3]:

$$f = \frac{1}{2} K (\Delta_\perp u)^2 + \frac{1}{2} B \left[ \frac{\partial u}{\partial z} - \frac{1}{2} (\nabla_\perp u)^2 \right]^2 - \frac{1}{2} \varepsilon_0 |\varepsilon_a| E^2 (\nabla_\perp u)^2, \quad (1)$$

where  $u(x, y, z)$  is a small displacement of layers from the reference flat state,  $\Delta_\perp u = \partial^2 u / \partial x^2 + \partial^2 u / \partial y^2$ , and  $(\nabla_\perp u)^2$

$= (\partial u / \partial x)^2 + (\partial u / \partial y)^2$ ; the elastic constants of splay ( $K$ ) and layers dilation ( $B$ ) can be expressed through the Frank elastic constants for bend  $K_3$  and twist  $K_2$  of the director as  $K = 3K_3/8$  and  $B = K_2(2\pi/p)^2$ , respectively [1,11].

### C. Finite surface anchoring energy

Layers deviations from the orientations parallel to the bounding plates are described by a coarse-grained cholesteric anchoring potential [52]

$$W_\chi = \frac{1}{2} W_{\chi 0} (\nabla_\perp u)^2, \quad (2)$$

where  $W_{\chi 0} = W_p/2$ ,  $W_p$  is the polar anchoring coefficient for  $\mathbf{n}$  [3,53]. Note that the surface anchoring is considered as azimuthally degenerate. Such an approach is generally not valid when the plates are unidirectionally treated (rubbed polyimide substrates), as the in-plane anchoring implies dilations of the cholesteric layers, when  $2d/p$  is not an integer (for parallel rubbing at two substrates). These dilations, however, are small, less than  $p/4d$ , and do not influence much the square symmetry of the ensuing deformations in the experiments. Thus the model with a degenerate in-plane anchoring is sufficient to capture the most essential features of undulations even when the plates are rubbed.

### D. Onset of undulations in softly anchored lamellae

The coarse-grained free energy of a cholesteric LC in an external field is [1,11,52]

$$F = \int_V f dV + \frac{1}{2} W_{\chi 0} \int_S \{ (\nabla_\perp u)_{z=-d/2}^2 + (\nabla_\perp u)_{z=d/2}^2 \} dS. \quad (3)$$

The layers displacement at  $E \gtrsim E_c$ , satisfying the corresponding Euler-Lagrange equation with the boundary conditions following from Eq. (3), is of the form [19,22,23,50]

$$u(x, y, z) = u_0 \cos q_z z \cos q_\perp x \cos q_\perp y \quad (4)$$

with the constraints

$$q_z = q_\perp \sqrt{2(\kappa - 2\lambda^2 q_\perp^2)}, \quad (5)$$

$$\frac{B}{W_{\chi 0}} = \frac{\sqrt{2} q_\perp \cot(q_\perp d \sqrt{(\kappa - 2\lambda^2 q_\perp^2)/2})}{\sqrt{\kappa - 2\lambda^2 q_\perp^2}}, \quad (6)$$

where  $q_\perp^2 = (q_x^2 + q_y^2)/4$ ,  $L_\perp = 2\pi/q_\perp$ ,  $q_x = 2\pi/L_x$ ,  $q_y = 2\pi/L_y$ , Fig. 1(d),  $\kappa = \varepsilon_0 |\varepsilon_a| E^2 / B$ , and  $\lambda = \sqrt{K/B}$  is the penetration length. The right-hand side of Eq. (6) is a function of  $q_\perp$  and  $\kappa$

$$g(q_\perp, \kappa) = \frac{\sqrt{2} q_\perp \cot(q_\perp d \sqrt{(\kappa - 2\lambda^2 q_\perp^2)/2})}{\sqrt{\kappa - 2\lambda^2 q_\perp^2}}. \quad (7)$$

For a given field ( $\kappa = \text{const}$ ) the function  $g(q_\perp)$  is symmetric with two minima, Fig. 2. Consider first the case of infinite anchoring,  $W_{\chi 0} \rightarrow \infty$ , denoting  $\kappa$  for this case as  $\kappa^\infty$ , and  $q_\perp$  as  $q_\perp^\infty$ . At low fields,  $g(q_\perp)$  is always positive, see the curve labeled  $\kappa^\infty = 0.8\kappa_c^\infty$  in Fig. 2(a). As the field increases and  $\kappa^\infty$

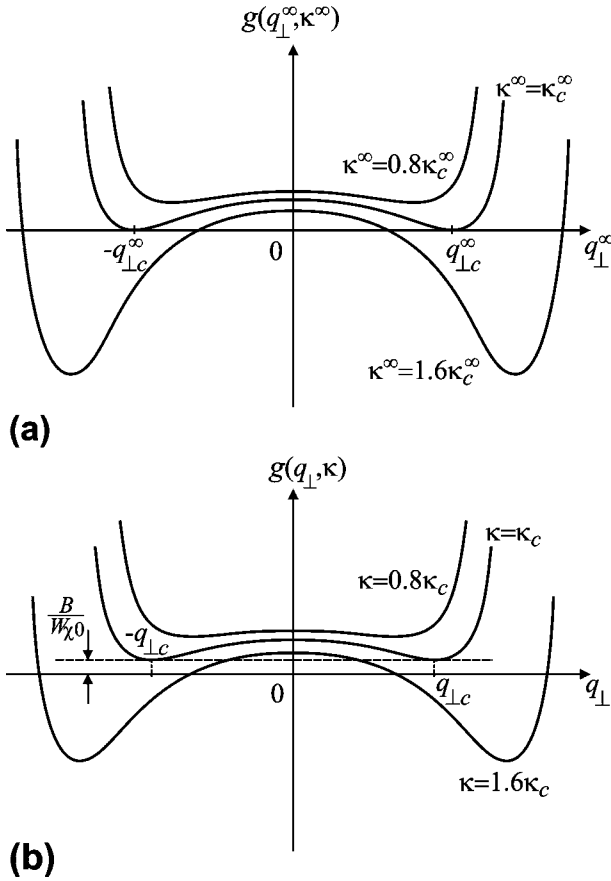


FIG. 2. Behavior of the function  $g(q_{\perp}, \kappa)$  at three different values of the applied electric field for the case of infinitely strong surface anchoring (a) and finite surface anchoring (b), as calculated from Eq. (7) for  $\lambda=0.7 \mu\text{m}$  and  $B/W_{\chi 0} \approx 0.2 \mu\text{m}^{-1}$ . The threshold fields correspond to  $\kappa_c^{\infty} \approx 0.084$  in (a) and  $\kappa_c \approx 0.075$  in (b).

reaches some threshold value  $\kappa_c^{\infty}$ , the ordinate of the two minima of  $g(q_{\perp}^{\infty})$  decreases to zero, Fig. 2(a), so that Eq. (6) with  $W_{\chi 0} \rightarrow \infty$  is satisfied for some  $q_{\perp}^{\infty} = \pm q_{\perp c}^{\infty}$ . The latter value is the critical wave number of undulations that become energetically preferable above the threshold electric field,  $\kappa^{\infty} > \kappa_c^{\infty}$ .

When the anchoring is not infinitely strong, the qualitative behavior of  $g(q_{\perp})$  remains the same, Fig. 2(b). The difference is that the threshold  $\kappa_c$  is achieved when the ordinate of the two minima of  $g(q_{\perp})$  reaches the value  $B/W_{\chi 0} > 0$  (rather than zero as in the case of infinite anchoring), so that Eq. (6) is satisfied for two points  $q_{\perp} = \pm q_{\perp c}$ . As follows from Eq. (6),  $\kappa_c = 2q_{\perp c}^2 \lambda^2 d / \alpha$ , so that the threshold electric field for the layers undulation in the 3D layered system is

$$E_c = q_{\perp c} \sqrt{\frac{2Kd}{\alpha \varepsilon_0 |\varepsilon_a|}} \quad (8)$$

with a constraint on the wave numbers found from Eq. (5) as

$$q_{\perp c}^2 = \frac{q_{zc}}{2\lambda} \left( \frac{\alpha}{\beta} \right)^{1/2}, \quad (9)$$

where  $q_{zc}$  is the threshold value of the wave number along the  $z$  direction, and

$$\alpha = \frac{d}{2} \left( 1 - \frac{\sin q_{zc} d}{q_{zc} d} \right) \quad \text{and} \quad \beta = \frac{d}{2} \left( 1 + \frac{\sin q_{zc} d}{q_{zc} d} \right) \quad (10)$$

are two parameters that depend on the ratio  $B/W_{\chi 0}$ .

In order to find the amplitude of undulations above the threshold, we now calculate the free energy density per one period of undulations with the displacement  $u$  [Eq. (4)] keeping the terms in Eq. (3) up to  $\sim u_0^4$ :

$$\frac{d\tilde{f}}{K} = \frac{q_{\perp}^4 d \beta}{4 \alpha} \left\{ 1 - \frac{E^2}{E_c^2} \right\} u_0^2 + \frac{5}{8192} \frac{q_{\perp}^2 \rho}{\lambda^3} \sqrt{\frac{\alpha}{\beta}} u_0^4, \quad (11)$$

where the dimensionless parameter

$$\rho = 6q_{zc} d + 8 \sin(q_{zc} d) + \sin(2q_{zc} d) \quad (12)$$

depends on the anchoring coefficient  $W_{\chi 0}$ .

Minimizing Eq. (11) with respect to  $u_0$ , one finds the maximum amplitude of undulations at  $E \gtrsim E_c$  and  $z=0$ , as

$$u_0 = \frac{4\lambda \gamma \eta}{\sqrt{3}} \left( \frac{E^2}{E_c^2} - 1 \right)^{1/2}, \quad (13)$$

where

$$\gamma = \frac{q_{xc}^2 + q_{yc}^2}{\left( q_{xc}^4 + \frac{2}{9} q_{xc}^2 q_{yc}^2 + q_{yc}^4 \right)^{1/2}} \left( \frac{2}{\sqrt{3}} \right)^n; \quad (14)$$

$$\eta = \sqrt{2} q_{\perp c} \left( \frac{6\lambda d}{\rho} \right)^{1/2} \left( \frac{\beta}{\alpha} \right)^{3/4}. \quad (15)$$

Here  $n=1$  corresponds to the 1D striplike undulation pattern in the 2D sample and  $n=2$  to the square lattice in the 3D sample;  $\eta$  depends on the anchoring coefficient  $W_{\chi 0}$ , Eqs. (10) and (12). For an infinitely strong surface anchoring  $\eta = 1$  and Eq. (13) reduces to the well-known form found in Refs. [19,37]. When the surface anchoring is finite, then  $\eta > 1$  and the displacement magnitude  $u_0$  increases [15,16], see Eq. (13). Equation (13) reproduces the results of Refs. [15,16] for  $n=1$  and  $q_{yc}=0$ .

### E. Undulations at high fields

At the onset of undulations, the displacement is sinusoidal, Eq. (4). As  $E$  increases well above  $E_c$ , the pattern adopts a zigzag shape. Singer [13,17] described this regime by neglecting the  $z$ -dependence of  $u$  in the center of the cell at higher fields. Clearly, such an assumption works even better if the surface anchoring at the bounding plates is not infinitely strong, as the layers at the boundaries can tilt together with the layers in the bulk, as observed experimentally for the 2D cholesteric system [16].

We follow the approach [13,16] and ignore the  $z$ -dependence of layers in the central part of the cell. For the square lattice with  $q_x = q_y$ , the free energy density (1) per unit area in the vertical  $lz$  plane, where  $l=x, y$ , is

$$f = \frac{Bd}{2} \left\{ 4\lambda^2 \left( \frac{\partial \theta}{\partial l} \right)^2 + \theta^4 - 2 \frac{\varepsilon_0 |\varepsilon_a| E^2}{B} \theta^2 \right\}. \quad (16)$$

The corresponding Euler-Lagrange equation

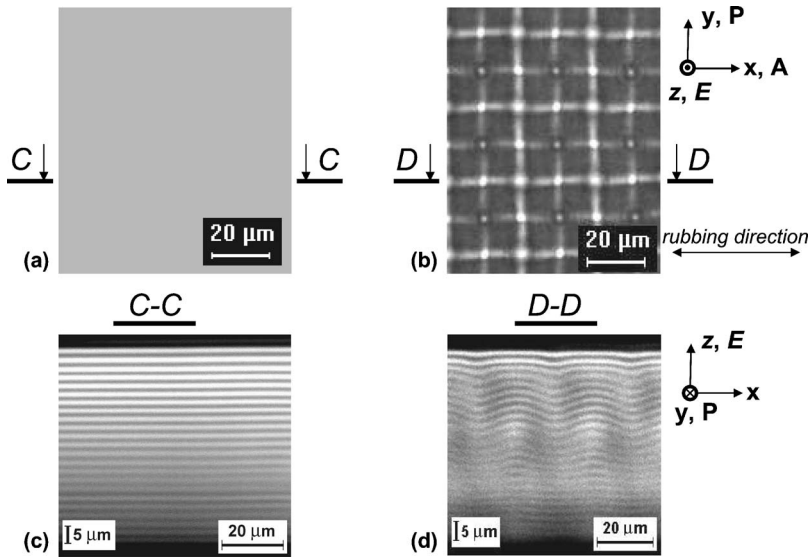


FIG. 3. Textures of a cholesteric cell of thickness  $d=55 \mu\text{m}$  ( $p=5 \mu\text{m}$ , alignment layer-PI2555), viewed by PM in the horizontal  $xy$  plane (a,b) and by FCPM in the vertical cross-section  $xz$  (c,d): (a,c) uniform structure,  $E=0$ ; (b,d) layer undulations at  $E>E_c$ ,  $E=1.05E_c$  ( $U \approx 12.5 \text{ V}$ ); “P” and “A” show the directions of light polarization transmission for the polarizer and analyzer, respectively;  $\mathbf{E}$  is the electric field.

$$\lambda^2 \frac{\partial^2 \theta}{\partial l^2} + \kappa' \theta - \frac{1}{2} \theta^3 = 0 \quad (17)$$

with  $\kappa' = \frac{\varepsilon_0 |\varepsilon_a| E^2}{2B}$  is of the same form as in Refs. [13,14,16]. Therefore the spatial dependence of the tilt angle is

$$\theta(l) = \theta_{max} \text{sn} \left( \frac{\sqrt{2\kappa - \theta_{max}^2} l}{2\lambda} \middle| m \right), \quad (18)$$

where  $\text{sn}(g|m)$  is the Jacobi elliptic function [54],  $m^2 = \frac{\theta_{max}^2}{2\kappa - \theta_{max}^2} < 1$  is the field-dependent parameter, and  $\theta_{max}$  is the maximum tilt angle of the layers [16]. The displacement  $u(l)$  is obtained by integrating Eq. (18)

$$u(l) = \frac{\theta_{max}}{A\sqrt{m}} \log[\text{dn}(Al|m) - \sqrt{m} \text{cn}(Al|m)] + \text{const}, \quad (19)$$

where  $A = \frac{\sqrt{2\kappa - \theta_{max}^2}}{2\lambda}$ ,  $\text{cn}(g|m)$  and  $\text{dn}(g|m)$  are the Jacobi elliptic functions [54]. In the limit  $m \rightarrow 0$ , the undulation profile  $u(l)$  is sinusoidal, while for  $m \rightarrow 1$  it is of a zigzag character with a longer period. As we shall see in Sec. IV, the experimental data on the 3D system are in a good agreement with these predictions and with the data for 2D systems [13,14,16].

### III. MATERIALS AND EXPERIMENTAL TECHNIQUES

#### A. Materials

The LC cells were assembled from glass plates coated with transparent indium tin oxide (ITO) electrodes. To study the role of surface anchoring we used different alignment materials. Thin films of polyimide PI2555 (HD MicroSystem) and poly(vinyl alcohol) (PVA; Aldrich Chemical Company, Inc.) aqueous (1 wt %) solution were used to provide the strong planar surface anchoring,  $W_p = (4 \pm 1) \times 10^{-4} \text{ J/m}^2$  [52]; the substrates were rubbed for better alignment (1–15 rubbings with pressure in the range 800–850 Pa). The alignment layers that produce weak planar anchoring were obtained with unrubbed thin films of spin-

coated polyisoprene (PI; Aldrich Chemical Company, Inc.) dissolved (1 wt %) in methylcyclohexane (Acros Organics),  $W_p = (0.7 \pm 0.6) \times 10^{-4} \text{ J/m}^2$  [52,55]. The cell thickness was set by glass spacers mixed with UV-light sensitive glue at the cell edges. The cells thickness was set within the range  $d = 50\text{--}70 \mu\text{m}$ . The actual  $d$  was measured using the interference method and spectrophotometer Lambda18 (Perkin Elmer). To minimize spherical aberrations in the FCPM observations [9] with immersion oil objectives, we used glass plates of thickness 0.15 mm with the refractive index 1.52.

One of the experimental challenges in the study of the undulations is that linear defects—bundles of dislocations and disclinations, called the oily streaks, destroy the planar state before the undulations pattern has a chance to develop [56]. These defects appear through nucleation [56], usually at the irregularities created by the edges of the cell. We found an effective way to avoid the oily streaks by patterning the ITO electrodes and reducing their area to only the central portion of the cell,  $\sim 5 \times 5 \text{ mm}^2$ , thus separating the edges of the undulations pattern from the edges of the cell.

The cholesteric mixture was prepared by doping the nematic host ZLI-3412-100 with the chiral additive CB15 (both from EM Industries) in weight proportion 96.83:3.17 to achieve the pitch  $p=5 \mu\text{m}$  (as measured by the Grandjean-Cano technique [51]). The material parameters of ZLI-3412-100, reported by the manufacturer, are as follows:  $\varepsilon_{\parallel}=7.3$ ,  $\varepsilon_{\perp}=4.2$ ,  $\Delta\varepsilon=3.4$ ; the extraordinary refractive index  $n_e=1.5578$ , the ordinary refractive index  $n_o=1.4798$ , birefringence  $\Delta n=0.078$ ; elastic constants  $K_1=14.1 \text{ pN}$  (splay),  $K_2=6.7 \text{ pN}$  (twist), and  $K_3=15.5 \text{ pN}$  (bend). For the FCPM studies [9], the cholesteric mixture was additionally doped with a small amount (0.01 wt %) of fluorescent dye  $n,n'$ -bis(2,5-di-*tert*-butylphenyl)-3,4,9,10-perylenedicarboximide (BTBP; Aldrich Chemical Company, Inc.), which does not affect the phase diagram and structure of the cholesteric LC [9]. The cells were filled with the cholesteric mixtures in the isotropic state and then slowly (0.5 deg/min) cooled down, to obtain a uniform planar structure, Fig. 1(b), 3(a), and 3(c). An ac voltage (1 kHz) was applied using the generator DS345 (Stanford Research Systems) and the wideband amplifier 7602 (Krohn-Hite).

TABLE I. Surface anchoring parameters.

Alignment material	$\eta$	Coarse-grained anchoring coefficient $W_{\chi_0}(\times 10^{-4} \text{ J/m}^2)$	Extrapolation length $\zeta(\mu\text{m})$	Critical field $E_c(\text{V}/\mu\text{m})$
PI2555 (15 rubbings <sup>a</sup> )	$1.56 \pm 0.5$	$(1.12 \pm 0.2)$	0.95	0.22
PVA (7 rubbings <sup>a</sup> )	$1.59 \pm 0.5$	$(0.29 \pm 0.2)$	2.24	0.20
PI2555 (7 rubbings <sup>a</sup> )	$2.04 \pm 0.5$	$(0.25 \pm 0.2)$	4.8	0.20
PI (no rubbing)	$3.59 \pm 0.5$	$(0.13 \pm 0.1)$	17.4	0.19

<sup>a</sup>Pressure  $\approx 800\text{--}850$  Pa.

### B. Imaging techniques

Polarizing microscopy observations were performed using a Nikon Eclipse E600 microscope equipped with a Hitachi HV-C20 CCD camera. The FCPM studies were performed using the modified BX-50 Olympus microscope [9]. By using the nematic host with low birefringence,  $\Delta n = 0.078$ , we mitigated the problem of beam defocusing and the Mauguin effect in the FCPM imaging [57,58]. The Ar laser ( $\lambda = 488$  nm) was used for excitation of the BTBP and the fluorescent light was detected in the spectral range 510–550 nm. It is important to note that in the FCPM images the registered fluorescence signal from the bottom of the cell can be weaker than from the top because of some light absorption, light scattering caused by director fluctuation, depolarization, and defocusing [9]. These effects are especially noticeable in thick cells,  $d = 50\text{--}70$   $\mu\text{m}$ , used in our experiments, which explains some asymmetry of the FCPM images of the vertical cross sections of the cells.

## IV. EXPERIMENTAL RESULTS AND DISCUSSION

### A. 3D imaging of layers profiles of undulations

When the electric field above the threshold  $E_c$  ( $E_c \sim 0.2$  V/ $\mu\text{m}$ , see Table I) is applied to the cholesteric cell, it transforms the planar texture, Figs. 3(a) and 3(c), into the 2D square type undulations pattern, Figs. 3(b) and 3(d). The directions of two mutually orthogonal wave vectors  $\mathbf{q}_x$  and  $\mathbf{q}_y$  of the periodic pattern depend on the type of the surface anchoring in the cells. For example, in the cells with orthogonal in-plane rubbing directions at the two opposite glass plates,  $\mathbf{q}_x$  and  $\mathbf{q}_y$  make an angle  $45^\circ \pm 10^\circ$  with the rubbing directions, remaining orthogonal to each other. The deviations from the direction  $45^\circ$  are more pronounced when  $d/p > 10$ ; for  $3 < d/p < 10$ , the deviations are normally less than  $3^\circ$ . In the cells with plates rubbed in an antiparallel fashion,  $\mathbf{q}_x$  and  $\mathbf{q}_y$  are parallel (perpendicular) to the rubbing directions. However, for all types of rubbing orientations, wave vectors remain orthogonal to each other and their absolute values are equal, as determined with an accuracy better than 1%, Fig. 3(b).

From PM textures, Fig. 3(b), one could assume that bright spots in the undulations pattern correspond to director singularities. However, the cross-sectional FCPM view of the undulations, Fig. 3(d), reveals no director singularities. The bright spots originate from the lensing effect of the undulat-

ing pattern. Really, for a light beam propagating across the cell through the regions where the layers have zero tilt, the index of refraction is maximum; for the regions with the highest tilt, the index of refraction is minimum. As a result, light is focused towards the regions with zero tilt of layers, compare Figs. 3(b) and 3(d), giving rise to bright lines and spots in Fig. 3(b).

The typical rise time of undulations in a cholesteric LC can be estimated following Ben-Abraham and Oswald [59] as  $\tau = \eta_{eff} \lambda d / K$ ; in our case, with  $\eta_{eff} \sim 0.1$  J s/m<sup>3</sup> as a characteristic viscosity,  $\lambda \approx 1$   $\mu\text{m}$  (as calculated from the values of  $K$  and  $B$  [60]),  $K = 3K_3/8 \approx 6$  pN, and  $d \approx 60$   $\mu\text{m}$ , the rise time is of the order of 1 s. We performed the experiments in a quasistatic regime when the rate of the field increase,  $\sim 50$  mV/min, was about four orders of magnitude smaller than the rate of undulations growth estimated as  $E_c d / \tau \sim 600$  V/min.

At the onset of undulations and for  $E$  close to  $E_c$ , the layers undulations along the  $x$  and  $y$  directions are clearly sinusoidal, as in Eq. (4), see Fig. 4. When  $E$  increases, the amplitude of buckling increases and the layers gradually adopt the zigzag shape, Fig. 5. The displacements become less dependent on  $z$  coordinate, Fig. 5(a), as in the case of 2D systems [15,16]. Equation (19) describes the experimental zigzag profiles very well, Figs. 5(a) and 5(b). The spatial periods  $L_x$  and  $L_y$  of the 2D square lattice increase with the field, Fig. 6(a), through the appearance and climb of edge dislocations with Burgers vector  $b = L_x, L_y$ , Fig. 6(b).

### B. Effect of finite surface anchoring

The appearance of sinusoidal distortions at  $E_c$  and their gradual transformation into zigzag shapes as the field increases above  $E_c$  are the common features of the undulation instability in all studied cells that remain qualitatively the same regardless of the type of (planar) alignment layers. However, the quantitative details show a strong dependence on the strength of surface anchoring that is different for different aligning layers.

First, the threshold of undulations  $E_c$  becomes lower as the polyimide coating PI2555 is replaced with PVA and then with polyisoprene PI alignment films, see Table I.

Second, the surface anchoring strongly influences the field dependence of layer displacements from the flat reference state. Using the FCPM, we measured the amplitude  $u_0$  of vertical displacement of the central layer, as the function of the applied field immediately above  $E_c$ . The experiment,

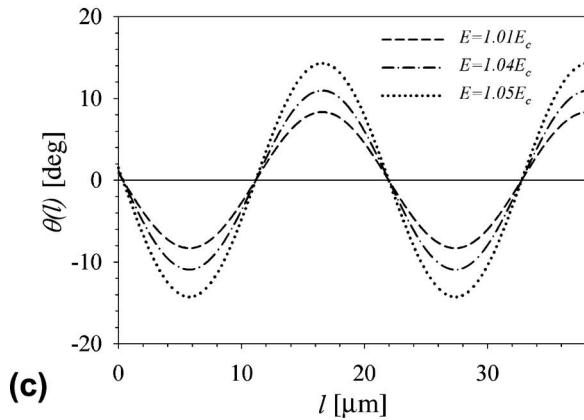
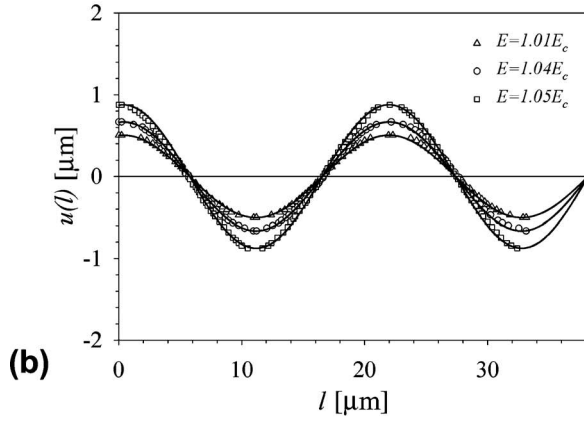
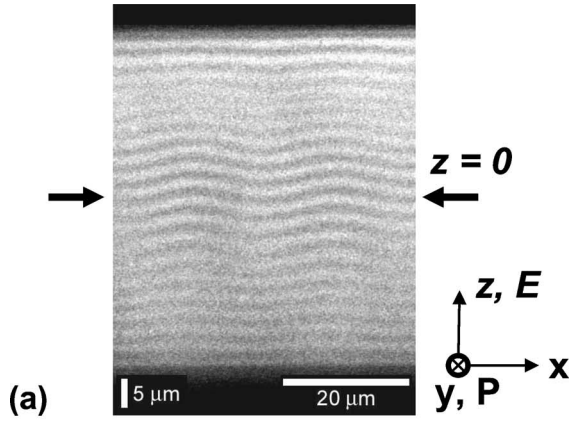


FIG. 4. (a) FCPM texture of sinusoidal undulation profile in the vertical cross section of a cholesteric cell of thickness  $d=50 \mu\text{m}$  at low fields,  $E=1.04E_c$ , (b) the vertical displacement and (c) the tilt angle of the undulating central layer ( $z=0$ ) as the function of the horizontal coordinate  $l=x, y$ , as deduced from the FCPM textures. In (b), the experimental data are fitted with Eq. (4) (solid lines); in (c), the dashed lines are derived from the experimental data in (b).

Figs. 4, 5, and 7 shows that for all studied alignment layers, the data are well-fitted by the expression that follows from Eq. (13),

$$u_0 = \frac{16}{\sqrt{15}} \lambda \eta \left( \frac{E^2}{E_c^2} - 1 \right)^{1/2}, \quad (20)$$

with the fitting values of  $\eta$  presented in Table I. Although for all types of alignment layers the trend  $u_0 \propto \sqrt{E^2/E_c^2 - 1}$  is the

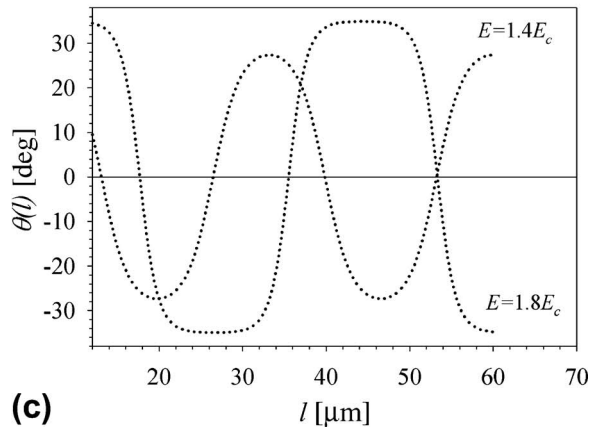
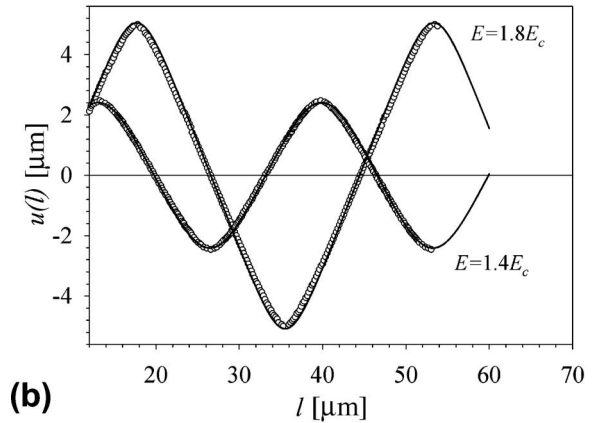
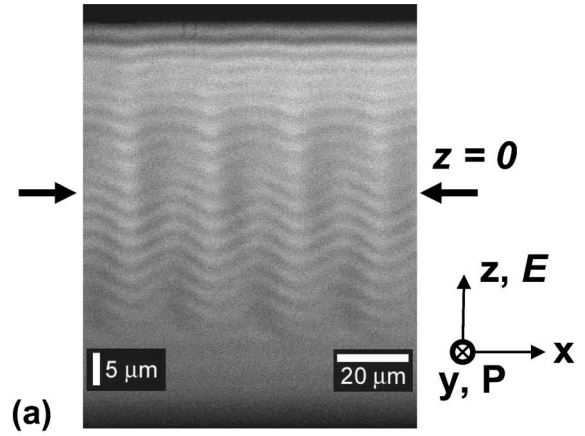


FIG. 5. (a) FCPM texture of sawtooth undulation profile in the vertical cross section of a cholesteric cell of thickness  $d=50 \mu\text{m}$  at elevated fields,  $E=1.4E_c$ , (b) the vertical displacement and (c) the tilt angle of the undulating central layer ( $z=0$ ) as the function of the horizontal coordinate  $l=x, y$ , as deduced from the FCPM textures at  $E=1.4E_c$  and  $E=1.8E_c$ . In (b), the experimental data are fitted with Eq. (19) (solid lines); in (c), the dotted lines are derived from the experimental data in (b).

same near the threshold, the slope  $\eta$  is significantly higher than the value  $\eta=1$  expected in the infinite-anchoring models. The typical fitting values of  $\eta$  are about 1.6 for alignment layers PI2555 and PVA with a relatively strong anchoring and reach 3.6 for the PI layers yielding a very weak anchoring. Qualitatively, the effect is clear: a weaker anchor-

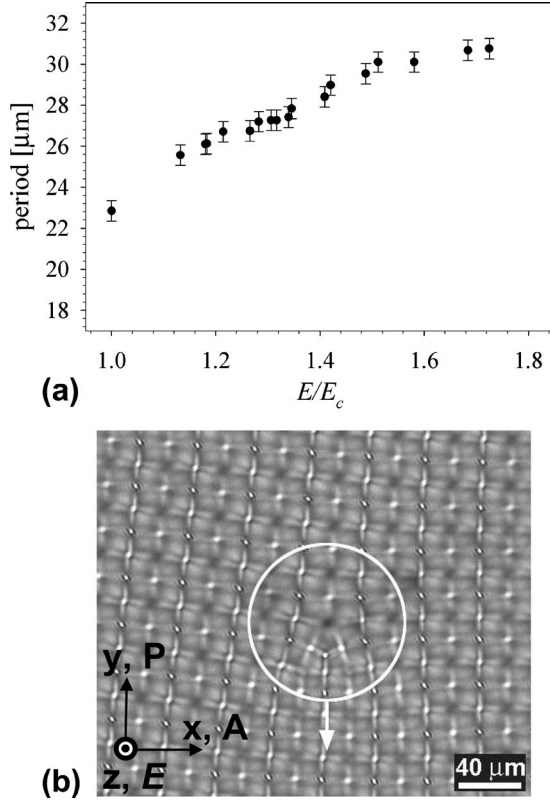


FIG. 6. (a) Undulation period  $L_x=L_y$  vs the applied field  $E/E_c$ ; (b) the undulation period is increased by a climb of an edge dislocation with Burgers vector  $b=L_x=L_y$ .

ing implies larger layers displacements  $u_0$  as the layers can tilt at the bounding plates. Quantitatively, we deduced the values of the polar anchoring coefficient  $W_{\chi_0}$  for different substrates, using the fitting (experimental) values of  $\eta$  and Eqs. (6), (10), (12), and (15) that relate  $\eta$  and  $W_{\chi_0}$ , in which

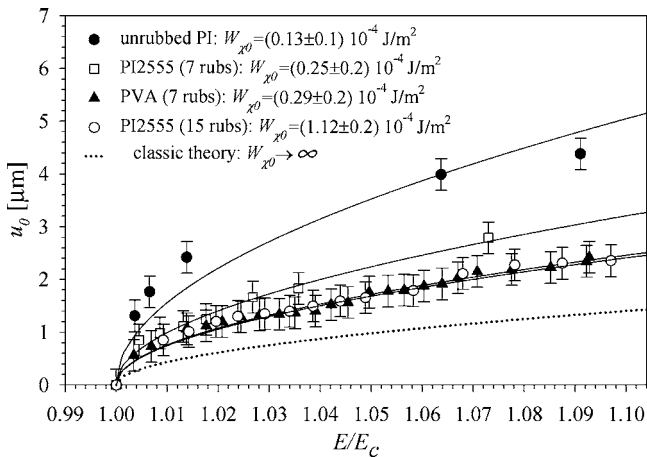


FIG. 7. Field dependence of layers displacement amplitude  $u_0$  in cells with different alignment layers as measured from the FCPM textures of the vertical cross sections of a cholesteric cell of thickness  $d=55 \mu\text{m}$ . The dotted line corresponds to the case of infinitely strong anchoring,  $W_{\chi_0} \rightarrow \infty$  ( $\eta=1$ ), Eq. (20). The experimental data are fitted with Eq. (20) for  $\eta>1$  (solid lines). The error bars are determined by the FCPM resolution in the vertical direction.

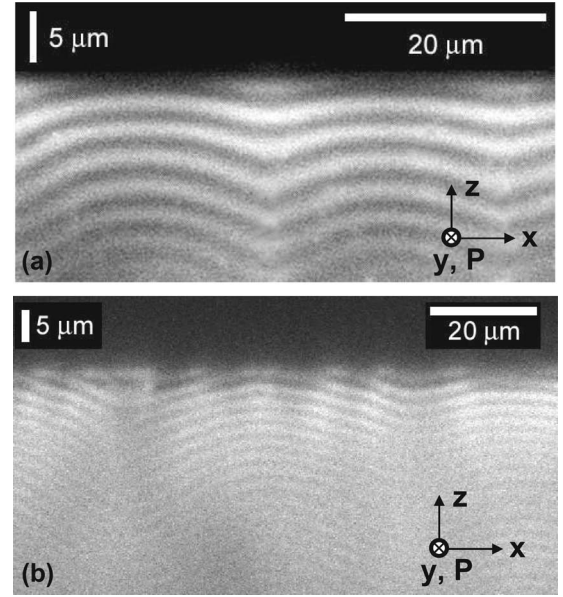


FIG. 8. FCPM textures demonstrating layers tilt in undulation patterns close to the boundaries coated with (a) rubbed film of PI2555 with strong anchoring; and (b) polyisoprene with weak anchoring. Both cells are of the same thickness  $d \approx 55 \mu\text{m}$ , filled with the same cholesteric mixture ( $p=5 \mu\text{m}$ ), and have the same field applied,  $E=1.1E_c$ .

$B=K_2(2\pi/p)^2 \approx 10 \text{ J/m}^3$ ,  $K \approx 5.8 \text{ pN}$ ,  $d \approx 60 \mu\text{m}$ , and  $p \approx 5 \mu\text{m}$ , see Table I. The values of  $W_{\chi_0}$  are of the same order of magnitude as those determined independently in Ref. [52]. Note that additional rubbing of PI2555 increases  $W_{\chi_0}$ ; a similar trend of the rubbing-induced increase of the polar anchoring coefficient  $W_p$  has been observed in the nematic LCs [61].

Third, a crucial feature of the layers buckling is that the displacement of the layers immediately adjacent to the bounding plates is definitely nonzero, Fig. 8, supporting the validity of the model with the finite surface anchoring. Figure 8 shows that the tilt of layers is relatively small near the boundaries with strong anchoring [PI2555 alignment layer, Fig. 8(a)] but becomes larger in the case of weak anchoring [unrubbed polyisoprene PI, Fig. 8(b)]. The layers adjacent to the surface adopt a nonsinusoidal profile even at weak fields, Fig. 8(a). The effect of finite surface anchoring can be qualitatively presented as an effective increase of the cell thickness,  $d \rightarrow d+2\zeta$ , over which the amplitude of undulations vanishes, Fig. 9, or, equivalently, as a decrease of the wave number  $q_z$ ,

$$q_z \approx \pi/(d+2\zeta). \quad (21)$$

Figure 9 shows the geometrical interpretation of the extrapolation length  $\zeta$  as well as the experimental data obtained for two cells with different surface anchoring. The experiment shows that  $\zeta$  increases when  $W_{\chi_0}$  decreases, from several micrometers for strong anchoring,  $W_{\chi_0} \approx (1.12 \pm 0.2) \times 10^{-4} \text{ J/m}^2$ , to tens of microns when  $W_{\chi_0} \approx (0.13 \pm 0.1) \times 10^{-4} \text{ J/m}^2$ , Figs. 8 and 9 and Table I.

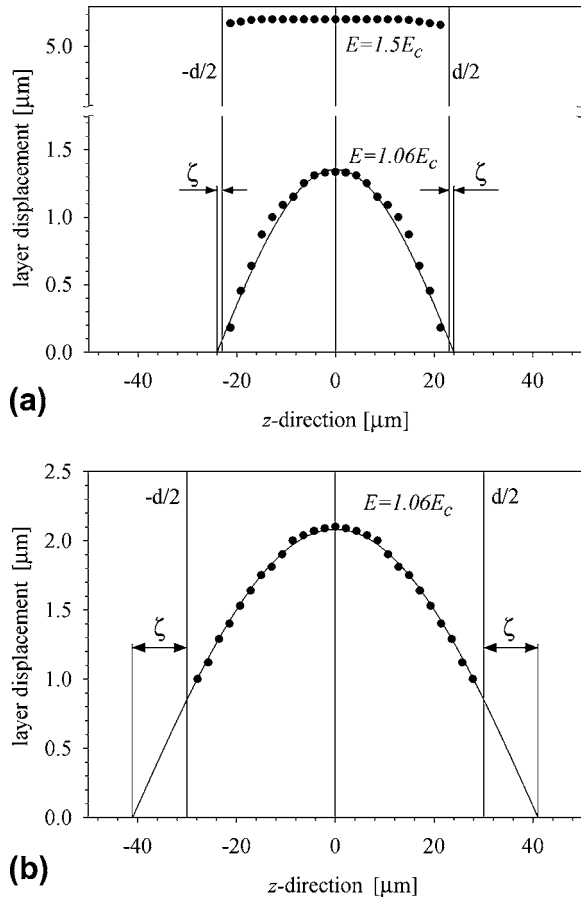


FIG. 9. Geometrical interpretation of the extrapolation length  $\zeta$  in the cell of thickness  $d$ : (a) the cell treated with PI2555 providing comparably strong surface anchoring,  $W_{\chi 0} = (1.12 \pm 0.2) \times 10^{-4} \text{ J/m}^2$ , at the boundaries; (b) the cell treated with PI providing weak surface anchoring,  $W_{\chi 0} = (0.13 \pm 0.1) \times 10^{-4} \text{ J/m}^2$ ; filled circles show the experimental data obtained from the FCPM textures; solid lines correspond to the best fit by  $u(z) = u_0 \cos(qz)$ .

### C. High-field unidirectional buckling with parabolic walls

As the applied electric field slowly ( $\sim 50 \text{ mV/min}$ ) increases to  $E \approx 1.8$  to  $1.9E_c$ , the undulations pattern changes one more time, as the 2D square lattice is replaced by a system of 1D stripes bounded by parabolic walls (PWs). The stripes with parabolic walls appear through a nucleation process that starts with the appearance of axially symmetric domains (ASDs), usually at the sites of surface imperfections, Fig. 10. When the ASD radius becomes comparable to  $d$ , it does not grow radially anymore, but transforms into a tip of growing stripe, Fig. 11(a). At a fixed voltage, the stripes

slowly ( $\approx 50 \mu\text{m/s}$  at  $E = 1.9E_c$ ) propagate replacing the original 2D square lattice of undulations, Fig. 11(b). Experimentally, the period  $L$  of the 1D stripe pattern is about two times larger than the period  $L_x$  of the square lattice and comparable to the cell thickness,  $L/d \approx 1$ . Even in the cells with rubbed substrates there was no preferred direction for the growth of 1D stripes within the 2D square lattice, Fig. 11(a). As would become clear from the discussion below, this is a natural consequence of the peculiar structure of stripes in which the layers near the boundaries are not tilted much and thus avoid the influence of in-plane surface anchoring.

The configuration of layers in stripes with PWs reconstructed from the 3D FCPM observations, Fig. 12(a), reveals that these structures are uniquely suited to balance the dielectric and surface anchoring forces, by combining titled layers in the bulk with practically horizontal layers near the boundaries. The tilted and flat horizontal portions of the layers join each other at two complementary sets of parabolic walls.

The observed texture can be qualitatively understood from the following geometrical consideration. At scales of deformations much larger than the period  $p/2$ , the lamellae can be approximated by a family of curved but equidistant surfaces. In the 2D plane (we consider it to be the plane normal to the stripe), there might be only two families of strictly equidistant flexible layers: concentric circles and flat layers. (In 3D, the curved layers are Dupin cyclides, i.e., surfaces whose lines of curvature are circles, see, e.g., Ref. [62]). Whenever a concentric packing of layers borders a flat configuration, the requirement of conservation of the number of layers implies that the boundary between the two families is a parabola, Fig. 13. Really, the conservation of layers implies that in Fig. 13,  $AM = MP$ , which is precisely the definition of a parabola; here  $M$  is a point on the parabola,  $A(0, h)$  is its focus (and the center of the concentric family of layers), and  $MP$  is the distance to the directrix of the parabola. A PW dividing the families of circular and flat layers has been already discussed in a model of a split core for dislocations of large Burgers vector [62].

In the stripe domains, the PWs appear in pairs, Fig. 12(b). The focus of one parabola serves as the end point of the oppositely oriented branch of the second parabola. The two parabolae of opposite orientation form a cigarlike region. Outside this cigarlike region, the layers are flat. Within the cigar region, there are two centers of layers curvature, namely, the two foci  $A$  and  $B$  of the complementary parabolae. The two families of circularly curved layers within the same cigar region match each other along the line  $AB$ : the circularly curved layers with the principal curvature  $1/R_B$  match the layers of a complementary family with the principal curvature  $1/R_A$  as they both cross  $AB$  normally, Fig. 12(b).

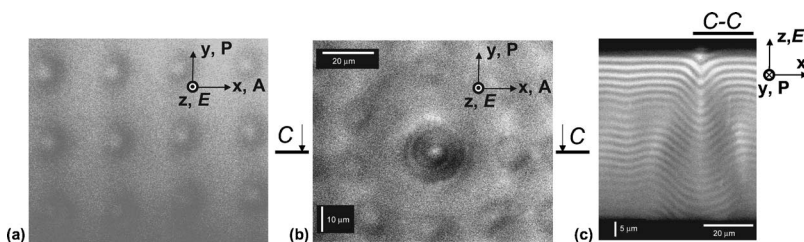


FIG. 10. Nucleation of ASDs: (a) FCPM in-plane view of the 2D square lattice of undulations; (b) FCPM in-plane view of the 2D square type undulations with a nucleated ASD; (c) FCPM vertical cross-section of the 2D square type undulations with a nucleated ASD; in all textures,  $E \approx 1.9E_c$ .

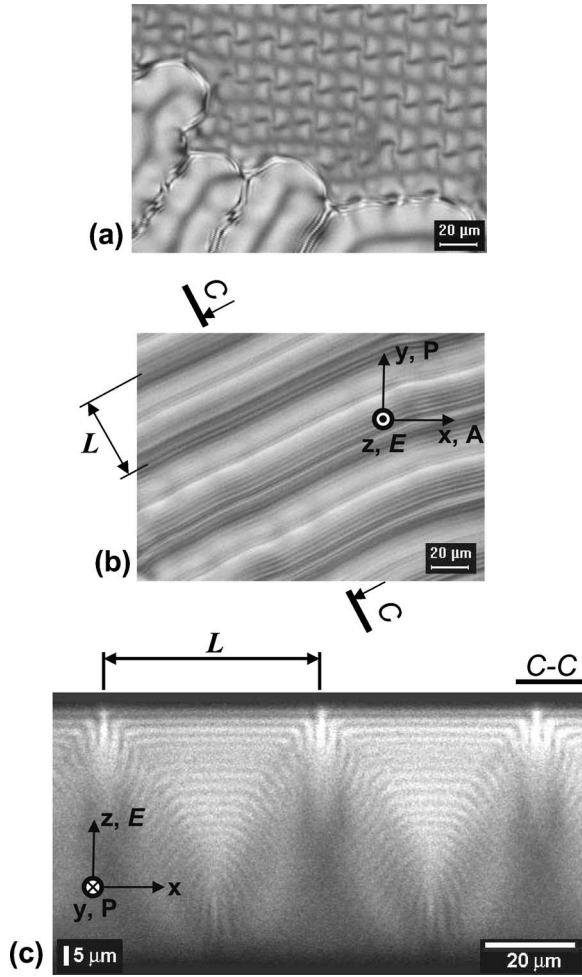


FIG. 11. Transformation of the 2D square lattice of undulations into the 1D stripe structure with PWs: (a) PM  $xy$  texture of propagating 1D stripes that replace the 2D lattice,  $E \approx 1.9E_c$ ; (b) PM  $xy$  texture of 1D stripe structure,  $E \approx 1.9E_c$ ; (c) FCPM vertical cross section of the 1D stripe structure with PWs, along the line  $C-C$  shown in (b).

The geometrical model in Fig. 12(b) captures the essential large-scale features of the stripe domains; however, at the scale of the pitch, the details are different. For example, the layer closest to the parabola focus is not cylindrical but forms a pair of disclinations with nonsingular cores,  $\lambda^{+1/2}$  and  $\lambda^{-1/2}$ , Figs. 11(c) and 12(a). The vertex of the parabola  $O$  is located at a finite distance  $p/2$  from the bounding plate, to accommodate for the nonsingular core of the  $\lambda^{-1/2}$  disclination, while the core of the  $\lambda^{+1/2}$  is at the parabola's focus, at the distance  $h \approx p/2$  from the vertex  $O$ . The geometrical model in Fig. 12(b) shows sharp cusps formed by the circular and flat layers merging at the parabolae, while in the real textures, Figs. 11(c) and 12(a), the cusps are blurred over the distances  $\sim p$ .

The main feature of the packing of layers in PWs structure is that the strongly tilted layers in the bulk coexist with the flat planar layers near the bounding substrates. Note that the ends of cigars rest near the boundaries of the cell; it means that the layers are parallel to the substrates practically everywhere, except near the cores of  $\lambda^{-1/2}$  disclinations. This

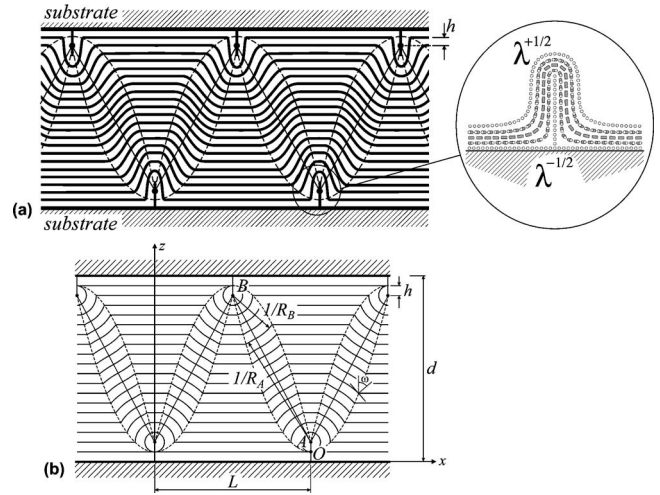


FIG. 12. (a) Configuration of layers in the stripe structure with parabolic walls (dashed lines) as reconstructed from the FCPM vertical cross-section textures of the cell; the solid lines corresponds to the regions where the director is perpendicular to the plane of figure; and (b) geometrical model of stripe structure. Filled circles show the foci of the parabolae that are also the centers of layers curvature. The inset in (a) shows the detailed director structure in the vicinity of two nonsingular  $\lambda$ -dislocations.

feature suggests that the main reason for the transformation of the 2D square lattice into the 1D PWs pattern is the finite surface anchoring, similar to the effect of focal conic domain-stripe transformation described in Ref. [63] for smectic A. Below we estimate the energy of the stripe domains and compare it to the possible anchoring energy of the zigzag configuration when the layers are strongly tilted at the boundaries.

The energy of a stripe structure, Fig. 12(b), calculated per unit length over the area  $Ld$ , is comprised of (a) the energy of four parabolic walls  $4F_{wall}^{PW}$ , (b) the dielectric energy, calculated with respect to the reference state with flat layers,  $4F_{el}^{PW}$ , where  $F_{el}^{PW}$  is calculated over the area restricted by one parabola segment, line  $AB$  and line  $OB$ , Fig. 12(b); (c) the energy of layers bend within the cigars regions  $F_{bend}^{PW}$  and (d) the core energies of the  $\lambda^{+1/2}$  and  $\lambda^{-1/2}$  disclinations. The last two contributions are of the order of  $\sim K$  and can thus be neglected as compared to  $F_{wall}^{PW}$  that is of the order of  $KL/\lambda$ , as shown below.

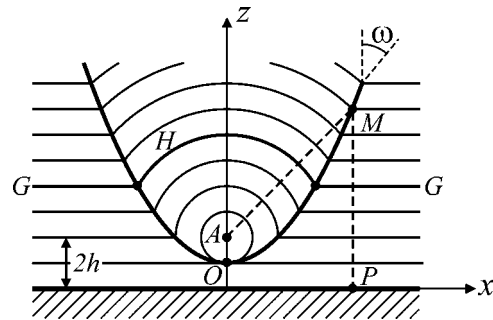


FIG. 13. Parabolic wall formed between a family of flat and circularly bent equidistant layers;  $AM=MP$ ;  $G$  and  $H$  are flat and bent portions of the same layer transversing the wall. The center of curvature of bent layers  $A$  is in the focus of the parabola.

Using the vertex equation of parabola,  $z=x^2/4h$ , we express the misalignment angle  $\omega$  between the tilted and flat layers at the wall as

$$\omega = \arctan \frac{4hx}{x^2 - 4h^2}. \quad (22)$$

The energy of the wall is then calculated by integrating the energy density per unit area of the wall [64]:

$$\sigma_{wall}^{PW} = \frac{2K}{\lambda} \left( \tan \frac{\omega}{2} - \frac{\omega}{2} \right) \cos \frac{\omega}{2}, \quad (23)$$

over the length of the wall:

$$F_{wall}^{PW} = \int_{h/2}^{L/2} \sigma_{wall}^{PW}(x) \sqrt{1 + z_x^2} dx, \quad (24)$$

where  $z_x^2 = x^2/4h^2$ . A straightforward calculation yields

$$F_{wall}^{PW} \approx \frac{KL}{\lambda}, \quad (25)$$

where we neglected the small terms  $\sim Kh/\lambda$  as  $h \ll L$ .

The dielectric energy  $F_{el}^{PW}$  is calculated as the double integral over half of the cigar region,

$$F_{el}^{PW} = -\frac{1}{2} \epsilon_0 |\epsilon_a| E^2 \int_0^{L/2} dx \int_{x^2/4h}^{h+2x(d-4h)/L} \sin^2 \gamma(x, z) dz, \quad (26)$$

where  $\gamma(x, z)$  is the angle between the field  $\mathbf{E}$  and local normal to the layers,  $\sin^2 \gamma = x^2/[x^2 + (z^2 - h^2)]$ ;  $\gamma = \omega$  at the parabolic walls. Neglecting the small terms  $\sim h/L$ , one arrives at

$$F_{el}^{PW} \approx -\frac{1}{16} \epsilon_0 |\epsilon_a| E^2 L^2 \arctan \frac{L}{2d}. \quad (27)$$

By balancing the elastic cost of the PWs and the dielectric gain from the layers tilt  $F_{el}^{PW} + F_{wall}^{PW} = 0$  at  $E = 1.9E_c$ , where  $E_c = \sqrt{\frac{2\pi K}{\epsilon_0 |\epsilon_a| \lambda d}}$  is approximated by its value in the infinite anchoring model, one can estimate roughly the ratio  $L/d \approx 1.2$ , which is close to the experimental value,  $L/d \approx 1$  at  $d = 55 \mu\text{m}$  and  $L = 50 \mu\text{m}$ .

Both the elastic and dielectric energy terms of the stripe structure are of the order of  $\sim KL/\lambda$ . The same order of magnitude is expected for the elastic and dielectric energies of the 2D zigzag pattern (the elastic term is caused by the domain walls separating regions with the opposite direction of layers tilt). However, in the 2D zigzag pattern, there is another significant contribution, caused by the layers tilt at the surfaces, Figs. 5 and 8. The anchoring energy density for large tilts is of the order of  $W_{\chi_0}$ . For the typical experimental values  $W_{\chi_0} \sim (0.1-1) \times 10^{-4} \text{ J/m}^2$ , it is comparable or larger than the elastic energy density carried by the PWs (or the walls in zigzag pattern),  $\sim 4F_{wall}^{PW}/L \sim 4K/\lambda \sim 0.4 \times 10^{-4} \text{ J/m}$ . Another possible texture, the lattice of parabolic

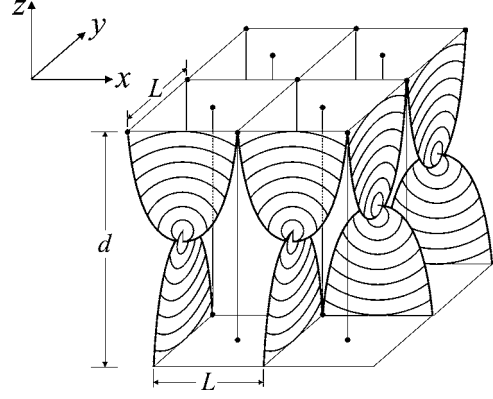


FIG. 14. PFC lattice with layers tilted at the boundaries.

focal conic domains (PFCs) [47], is also accompanied by a significant anchoring energy, as the layers are tilted at the boundaries, Fig. 14. We thus expect that the appearance of the stripe structure with PWs at the expense of both the 2D patterns of zigzag undulations and PFCs is related to the phenomenon of surface anchoring. Note, however, that in very thick samples (as compared to the period of the lamellar phase and to the period of the PFC lattice itself), the PFC structure with line defects but no walls might become a preferable one, as the anchoring energy density would scale as  $W_{\chi_0}(L/d)^2$  where  $L/d \ll 1$  determines the angle of surface misalignment, Fig. 14.

## V. CONCLUSIONS

Using the FCPM, we performed experimental studies of the scenario of layers undulations, or Helfrich-Hurault effect, in a 3D lamellar system, represented by a short pitch cholesteric liquid crystal. We study in detail how the shape of layers evolves in the applied field that tends to realign the layers from being horizontal and parallel to the bounding plates to being vertical and parallel to the applied field. The reorientation starts at a well-defined threshold field  $E_c$  with the layers adopting first a sinusoidal profile and then gradually changing to zigzag shapes with the increasing field. At  $E \gtrsim 1.9E_c$ , the 2D patterns of zigzag undulations transform into a 1D structure of stripes with parabolic defect walls.

We demonstrate that both the qualitative and quantitative features of undulations strongly depend on the surface anchoring at the cell boundaries. The finite surface anchoring at the plates decreases the threshold field  $E_c$  of undulations and allows for the much larger layer displacements and tilts above  $E_c$ , as compared to the classic theory with an infinite surface anchoring [4,5]. The FCPM textures of the vertical cross sections of the cell clearly demonstrate that the layers can tilt at the bounding plates. We extend the undulation model to the case of finite surface anchoring and use it to deduce the values of the surface anchoring coefficient at different aligning substrates by fitting the experimental data on field dependence of the layers displacements. At high fields, the 1D pattern of stripes with parabolic walls allows the layers to be tilted in the bulk but to remain parallel to the

bounding walls, thus avoiding a large energy associated with surface anchoring.

The present work deals with a quasistatic regime of undulation development. This scenario is expected to be different when the field is applied abruptly [22]. The studies of undulation dynamics are in progress.

## ACKNOWLEDGMENTS

We acknowledge support from Grant Nos. NSF DMS-0456221 and NSF DMR-0504516. We thank M. Kleman, T. Ishikawa, V. Pergamenschchick, S. Shiyonovskii, Yu. Nas-tishin, and L. Longa for discussions.

- 
- [1] P. G. de Gennes and J. Prost, *Physics of Liquid Crystals*, 2nd ed. (Clarendon Press, Oxford, 1992).
- [2] P. M. Chaikin and T. C. Lubensky, *Principles of Condensed Matter Physics* (Cambridge University Press, Cambridge, 1995).
- [3] M. Kleman and O. D. Lavrentovich, *Soft Matter Physics: An Introduction* (Springer, New York, 2003).
- [4] W. Helfrich, Appl. Phys. Lett. **17**, 531 (1970).
- [5] W. Helfrich, J. Chem. Phys. **55**, 839 (1971).
- [6] N. A. Clark and R. B. Meyer, Appl. Phys. Lett. **22**, 493 (1973); N. A. Clark and P. S. Pershan, Phys. Rev. Lett. **30**, 3 (1973).
- [7] M. Delaye, R. Ribotta, and G. Durand, Phys. Lett. **44A**, 139 (1973).
- [8] J. R. Bellare, H. T. Davis, W. G. Miller, and L. E. Scriven, J. Colloid Interface Sci. **136**, 305 (1990).
- [9] I. I. Smalyukh, S. V. Shiyonovskii, and O. D. Lavrentovich, Chem. Phys. Lett. **336**, 88 (2001).
- [10] I. I. Smalyukh, B. I. Senyuk, M. Gu, and O. D. Lavrentovich, Proc. SPIE **5947**, 594707 (2005).
- [11] T. C. Lubensky, Phys. Rev. A **6**, 452 (1972).
- [12] M. Zapotocky, L. Ramos, Ph. Poulin, T. C. Lubensky, and D. A. Weitz, Science **283**, 209 (1999).
- [13] S. J. Singer, Phys. Rev. E **48**, 2796 (1993).
- [14] R. E. Geer, S. J. Singer, J. V. Selinger, B. R. Ratna, and R. Shashidhar, Phys. Rev. E **57**, 3059 (1998).
- [15] T. Ishikawa and O. D. Lavrentovich, Phys. Rev. E **63**, 030501(R) (2001).
- [16] T. Ishikawa and O. D. Lavrentovich, in *Defects in Liquid Crystals: Computer Simulations, Theory and Experiments*, edited by O. D. Lavrentovich, P. Pasini, C. Zannoni, and S. Zumer, *NATO Science Series* (Kluwer Academic Publishers, Dordrecht, 2001).
- [17] S. J. Singer, Phys. Rev. E **62**, 3736 (2000).
- [18] D. R. M. Milliams and F. C. MacKintosh, Macromolecules **27**, 7677 (1994).
- [19] A. G. Zilman and R. Granek, Eur. Phys. J. B **11**, 593 (1999).
- [20] R. Bartolino and G. Durand, Phys. Rev. Lett. **39**, 1346 (1977).
- [21] R. Ribotta and G. Durand, J. Phys. (France) **38**, 179 (1977).
- [22] J.-I. Fukuda and A. Onuki, J. Phys. II **5**, 1107 (1995); J. Fukuda and A. Onuki, Macromolecules **28**, 8788 (1995).
- [23] I. W. Stewart, Phys. Rev. E **58**, 5926 (1998).
- [24] G. Bevilacqua and G. Napoli, Phys. Rev. E **72**, 041708 (2005).
- [25] I. W. Stewart, Liq. Cryst. **30**, 909 (2003).
- [26] T. J. Scheffer, Phys. Rev. Lett. **28**, 593 (1972).
- [27] F. Rondelez, H. Arnold, and C. J. Gerritsma, Phys. Rev. Lett. **28**, 735 (1972).
- [28] F. Rondelez and J. P. Hulin, Solid State Commun. **10**, 1009 (1972).
- [29] J. P. Hurault, J. Chem. Phys. **59**, 2068 (1973).
- [30] H. Hervet, J. P. Hurault, and F. Rondelez, Phys. Rev. A **8**, 3055 (1973).
- [31] J. M. Delrieu, J. Chem. Phys. **60**, 1081 (1974).
- [32] H. Arnould-Netillard and F. Rondelez, Mol. Cryst. Liq. Cryst. **26**, 11 (1974).
- [33] V. G. Chigrinov, V. V. Belyaev, S. V. Belyaev, and M. F. Grebenkin, Sov. Phys. JETP **50**, 994 (1979).
- [34] N. Scaramuzza, R. Bartolino, and G. Barbero, J. Appl. Phys. **53**, 8593 (1982); N. Scaramuzza, R. Barbero, F. Simoni, F. Xu, G. Barbero, and R. Bartolino, Phys. Rev. A **32**, 1134 (1985).
- [35] A. Leforestier and F. Livolant, J. Phys. II **2**, 1853 (1992); I. I. Smalyukh, O. V. Zribi, J. C. Butler, O. D. Lavrentovich, and G. C. L. Wong, Phys. Rev. Lett. **96**, 177801 (2006).
- [36] C.-M. Chen and F. C. MacKintosh, Phys. Rev. E **53**, 4933 (1996).
- [37] Z.-G. Wang, J. Chem. Phys. **100**, 2298 (1994).
- [38] Y. Cohen, R. J. Albalak, B. J. Dair, M. S. Capel, and E. L. Thomas, Macromolecules **33**, 6502 (2000); Y. Cohen, M. Brinkmann, and E. L. Thomas, J. Chem. Phys. **114**, 984 (2001).
- [39] M. Warner and E. M. Terentjev, *Liquid Crystal Elastomers* (Clarendon Press, Oxford, 2003).
- [40] M. D. Kempe, N. R. Scruggs, R. Verduzco, J. Lal, and J. A. Kornfield, Nat. Mater. **3**, 177 (2004).
- [41] F. Elias, C. Flament, J.-C. Bacri, and S. Neveu, J. Phys. I **7**, 711 (1997).
- [42] P. Molho, J. L. Porteseil, Y. Souche, J. Gouzerh, and J. C. S. Levy, J. Appl. Phys. **61**, 4188 (1987).
- [43] M. Seul and R. Wolfe, Phys. Rev. Lett. **68**, 2460 (1992); Phys. Rev. A **46**, 7519 (1992); **46**, 7534 (1992).
- [44] P. Poncharal, Z. L. Wang, D. Ugarte, and W. A. de Heer, Science **283**, 1513 (1999).
- [45] E. Cerda and L. Mahadevan, Phys. Rev. Lett. **90**, 074302 (2003); F. Brochard-Wyart and P. G. de Gennes, Science **300**, 441 (2003).
- [46] P. Oswald, G. C. Géminard, L. Lejček, and L. Sallen, J. Phys. II **6**, 281 (1996).
- [47] Ch. S. Rosenblatt, R. Pindak, N. A. Clark, and R. B. Meyer, J. Phys. (France) **38**, 1105 (1977).
- [48] W. J. Benton, E. W. Toor, C. A. Miller, and T. Fort, Jr., J. Phys. (France) **40**, 107 (1979).
- [49] S. A. Asher and P. S. Pershan, J. Phys. (France) **40**, 161 (1979).
- [50] S. A. Pikin, *Structural Transformations in Liquid Crystals* (Gordon and Breach Science Publishers, New York, 1991).
- [51] L. M. Blinov and V. G. Chigrinov, *Electrooptic Effects in Liquid Crystal Materials* (Springer, New York, 1994).
- [52] I. I. Smalyukh and O. D. Lavrentovich, Phys. Rev. Lett. **90**,

- 085503 (2003); in *Topology in Condensed Matter*, edited by M. Monastyrsky (Springer, Berlin, 2006), pp. 205–250.
- [53] A. Rapini and M. Papoular, *J. Phys. (Paris), Colloq.* **30**, C4-54 (1969).
- [54] M. Abramowitz and I. A. Stegun, *Handbook of Mathematical Functions with Formulas, Graphs, and Mathematical Tables* (Dover Publications, Inc., New York, 1972).
- [55] O. O. Ramdane, P. Auroy, S. Forget, E. Raspaud, P. Martinot-Lagarde, and I. Dozov, *Phys. Rev. Lett.* **84**, 3871 (2000).
- [56] O. D. Lavrentovich and D.-K. Yang, *Phys. Rev. E* **57**, R6269 (1998).
- [57] S. V. Shiyankovskii, I. I. Smalyukh, and O. D. Lavrentovich, in *Defects in Liquid Crystals: Computer Simulations, Theory and Experiments*, edited by O. D. Lavrentovich, P. Pasini, C. Zanoni, and S. Zumer, *NATO Science Series* (Kluwer Academic Publishers, Dordrecht, 2001).
- [58] I. I. Smalyukh and O. D. Lavrentovich, *Phys. Rev. E* **66**, 051703 (2002).
- [59] S. I. Ben-Abraham and P. Oswald, *Mol. Cryst. Liq. Cryst.* **94**, 383 (1983).
- [60] T. Ishikawa and O. D. Lavrentovich, *Phys. Rev. E* **60**, R5037 (1999).
- [61] D. S. Seo, *Liq. Cryst.* **26**, 1615 (1999).
- [62] M. Kleman, *Points, Lines and Walls: in Liquid Crystals, Magnetic Systems and Various Ordered Media* (Wiley, Chichester, 1983).
- [63] Z. Li and O. D. Lavrentovich, *Phys. Rev. Lett.* **73**, 280 (1994).
- [64] C. Blanc and M. Kleman, *Eur. Phys. J. B* **10**, 53 (1999).